Environmental and Climate Technologies
2025, vol. 29, no. 1, pp. 784–796
https://doi.org/10.2478/rtuect-2025-0052
https://content.sciendo.com

1862
RIGA TECHNICAL UNIVERSITY

Modelling and Experimental Characterization of Ice Storage for State of Charge Determination

Christian WAGNER[1*], Gayaneh ISSAYAN[2]

[1,2]*Research Group ASIC, University of Applied Sciences Upper Austria, Stelzhamerstrasse 23, 4600 Wels, Austria*

Received 11.04.2025; accepted 08.09.2025

Abstract **– The present surge in the popularity of ice storage applications has prompted research communities to dedicate efforts to the development of adequate and precise control strategies. Nevertheless, determining the state of charge (SoC) of the ice storage systems continues to present a considerable challenge. This publication explores the validity of determining the SoC of water-based latent heat storage employing capacitive sensors by taking advantage of the significant permittivity difference of liquid and solid phases. It does so by comparing the results of latter sensor with the simulation results of modelled storage. The innovative configuration of the heat exchanger exhibits a resemblance to a stainless-steel spiral coil and combines both plate and tube types. A series of measurements were conducted to collect data on the storage system's operational modes as part of the scope of this work. The experimental results of the capacitive SoC were then compared to those from the simulation model. The model is based on a one-dimensional energy balance using temperature dependent fluid properties for the calculation of the SoC of the ice storage. Preliminary validation results indicated a substantial agreement between the two sets, therefore enabling the formulation of further recommendation for operation of the ice storage system.**

Keywords **– Capacitive measurement; heat transfer; Phase Change Material (PCM); State of Charge (SoC); Thermal Energy Storage (TES).**

Nomenclature

A_{tr}	Heat transfer area	m^2
c_p	Specific heat	J/(kgK)
HEX	Heat exchanger	–
HTF	Heat transfer fluid	–
$\dot{m}$	Mass flow	kg/s
N	Total number of nodes	–
PCM	Phase change material	–
SoC	State of charge	–
T	Temperature	°C
TES	Thermal energy storage	–
U	Heat transfer coefficient	W/(m²K)
V	Volume	m^3

* Corresponding author.
E-mail address: christian.wagner@fh-wels.at

$\dot{V}_{in}$	Volume flow	L/h
ρ	Density	kg/m^3

1. INTRODUCTION

In tackling various challenges of the renewable energy transition ice storage systems are gaining on importance as versatile and efficient additions to heating and cooling systems. The flexibility of ice storage systems comprises of their dual utilization modes in heating and cooling [1], as well of the ability to be combined with heat pumps [2], [3] or solar thermal systems [4]. Ice storages belong to the group of latent energy storages (TES), where the latent heat during the phase change of a material can be utilized for to store energy. In contrast, sensible TES, such as conventional hot water tanks, store energy by using the sensible heat of the storage medium, which results in an increase of the storage medium's temperature. Latent TES in general, offer the advantage that a significant amount of heat can be stored using the latent heat of the phase transition. Ice storages use water as phase change material (PCM). Water/ice-systems therefore profit from low-cost, abundant, non-toxic material properties and high energy density [1]. To illustrate, an energy quantity of 334 kJ/kg is required or released to facilitate the phase change form ice to water or vice versa [5]. In comparison, with this specific amount of energy, one kilogram of water could be heated from 0 °C to 80 °C.

However, the use of latent TES introduces a series of challenges. One of the primary challenges in this context is determining the SoC of the storage. Knowledge of the SoC is not only essential for optimum operation of the TES itself, but also for the entire extended energy system [6]. The SoC of sensible TES can be easily determined by a simple temperature measurement of the storage medium. The SoC determination in sensible TES by temperature measurement is straightforward and very cost-effective, but not sufficient for latent storage applications. During the phase transition, the presence of both solid and liquid fractions of the PCM is observed. Furthermore, the temperature of the PCM remains theoretically constant. Consequently, the measurement of temperature is not a viable option in this case.

A growing body of literature has therefore examined different methods for estimating and measuring the SoC respectively the share of solid and liquid volume of latent TES. Steinmaurer *et al.* [7] used pressure sensors to register a change in air pressure due to the volumetric change of the PCM during phase transition in a closed system. They also attempted to calculate the SoC from integrating charging and discharging energies from the heat exchanger (HEX). However, this method requires precise knowledge of the heat losses that occur. Due to the estimation of heat losses, this method becomes inaccurate as errors accumulate over time [7]. Another possibility that has been investigated is based on the electrical conductivity of the PCM. Ezan *et al.* [8] developed a measurement method, which uses the significant change of electrical conductivity of the PCM during phase transition. In experimental results they achieved an accuracy of 3 %, compared to the photography method, where the thickness of a pipe's ice layer is scaled up from photographs by means of the pipe diameter [8]. In [9] the authors analysed different approaches for SoC determination and classified them after local or global measurement of the SoC.

For optimal operation of energy storages in general, knowledge of the dynamic behaviour is essential. While (quasi) steady state models of energy storages are frequently used for the optimization of large systems, for example as seen in [10], this approach is not appropriate for the optimization of the energy storage itself. Due to the time-dependent behaviour, especially with latent TES, the consideration of dynamic processes is inevitable for optimal operation. This includes for example, the allowance of the change of heat transfer coefficients, the change of thermodynamic properties or the kinetic of phase transition. However, the physical modelling of the phase transition presents a considerable challenge.

State of the art in modelling dynamic heat transfer processes in detail is using computational fluid dynamics (CFD) simulations [11]. Three-dimensional (3D) CFD-simulations enable a precise representation of heat transfer and physical processes, but they also result in a high computing time, which is not suitable for modelling entire energy systems with energy storages. Therefore, the use of two-dimensional (2D) or one-dimensional (1D) models for energy storages is a common approach when reduced computing time is required.

Barz *et al*. [12] developed a 2D-dynamic model with a linear state observer for estimating the SoC of a PCM-energy storage, which can be used for entire system simulations including model-based control methods. Carbonell *et al*. [4] used a 1D-energy equation model for simulating a ground-buried ice-storage over a one-year period. In [13] the authors presented a 1D mathematical model of a PCM-storage, which can be easily implemented into other models for system simulations. Bastida *et al*. [14] developed a 1D-discret dynamic model of an ice storage using temperature dependent fluid properties for the dynamic calculation of heat transfer coefficients and heat fluxes. Chengjun *et al*. [5] created a fast 1D numerical model for investigating the melting and icing process in an ice storage. In [15] the authors presented a method for estimating the SoC of latent TES using a non-linear state observer based on a 1D-model of the energy storage.

In this paper, a model based on the work of [14] is used to describe the heat transfer processes and calculate the SoC of an ice storage using stainless steel cooling bundles as HEX. In addition to the simulation work, the capacitive method is selected to measure the SoC of the storage. Determination of ice layer thickness and ice growth monitoring using capacitive sensing methods have been demonstrated by multiple groups [16], [17]. The measurement principle behind the mentioned method is based on the dielectric properties of water and ice. The spectra consist of $\varepsilon'(\omega)$ and $\varepsilon''(\omega)$ for real and imaginary terms of the dielectric permittivity of water and ice. For both phases, the $\varepsilon'(\omega)$ resembling a step downwards and $\varepsilon''(\omega)$ a peak, were found to be very similarly shaped, however shifted by six decades on the logarithmic frequency ω-scale [18]–[20]. The anomaly is also described by the Debye relaxation time of approximately 10^{-4} s for ice and 10^{-10} s for water coexisting at 0 °C [21]. Meaning that water and ice exhibit roughly equal relative permittivity for low frequency excitations, however, at higher frequencies of approximately 100 kHz and above that of ice decreases abruptly [22]. This simple and well-pronounced difference in the permittivity allows the capacitive sensing methods to be utilized.

This work concludes the preliminary SoC-investigations of an ice storage system equipped with a capacitive sensor. The phase change and crystallization of the ice layer on the HEX are modelled numerically and thereafter compared with the experimental findings.

2. Methods and Methodology

This work can be divided in two packages, which are described in the following sections. The first being the mathematical modelling of an ice storage system, which leads to the simulation. Followed by the second part, consisting of assembling the setup and fundamentals of the experimental characterization of the system.

2.1. Modelling and Simulation

After a comprehensive review of the available literature, it was determined that the modelling approach outlined in [14] is an appropriate fundament for the modelling activities carried out in scope of this work. The following therefore briefly describes the modelling approach in [14] and discuss the changes and modifications made in scope of this work. The model was designed for a water-based latent TES, where the HEX in the storage tank is made up of pairs of polyethylene tubes. The tubes are arranged in a spiral pattern in a counter-flow direction. The model can be reduced to a single pair of pipes, rather than simulating all the tubes in the storage, assuming a uniform temperature distribution over the height of the storage and a uniform flow within the tubes. The tubes are subsequently divided into discrete volume elements or nodes. A 1D energy balance is applied to each node, describing the energy flow due to the mass flow through the tubes and the heat exchange through the tube walls. Four differential equations are therefore required for each node (two equations for the supply flow tube and two equations for the return flow tube). The temperature dependence of fluid properties can be taken into account by the implementation of polynomial functions used to calculate thermodynamic fluid properties such as density or dynamic viscosity. This allows dynamic calculation of heat transfer coefficients and heat flows. The use of probability density functions to describe the specific heat and enthalpy allows to model the phase transition directly from the calculated temperature of the control volume. For a detailed view on the mathematical modelling see [14].

The modelling approach described above is used as basis for the modelling activities in scope of this work due to its flexible applicability and adaptability, as well as its suitability for carrying out system simulations. The model is based on the energy balance applied to a control volume, see Fig. 1.

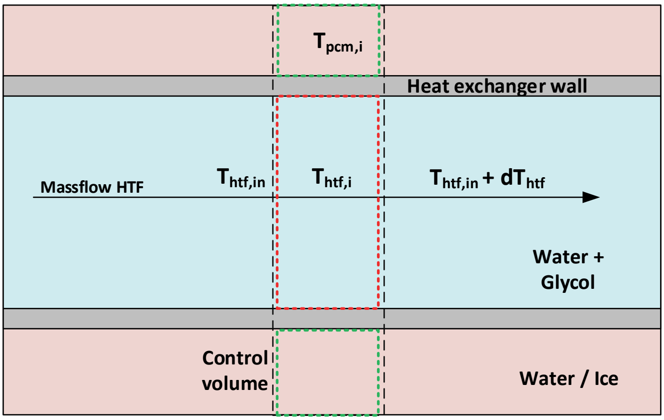

Fig. 1. Considered control volume (black dashed frame) consist of partial volume of the PCM (green dashed frame) and of a partial volume of the HTF (red dashed frame) as well as the HEX wall [own illustration adapted from [15]].

The control volume is made up of a partial volume of the PCM, a partial volume of the heat transfer fluid (HTF) and the HEX wall. Since in this model all HEX elements have parallel flow in the same direction and assuming that there are no heat losses, the number of differential equations per node can be reduced from four in the original model to two in the present case. For a sum of N considered control volumes or nodes, the energy balance results in a system of ordinary differential equations according to Eq. (1). The first row of the matrix describes the energy balance for the partial control volume of the HTF, including the energy transport due to the mass flow of the HTF and the heat flux through the HEX wall. The second row describes the energy balance for the partial control volume of the PCM, where only the heat flux through the wall of the HEX is considered.

Temperature dependent thermodynamic fluid properties are used for the dynamic calculation of heat transfer coefficients and heat flows. For the HTF usually a water-glycol mixture is used. However, the use of polynomial functions to determine the thermodynamic fluid properties is only valid for a certain defined mixing ratio of the HTF. In order to keep the model as flexible as possible, the fluid properties are not calculated using polynomial functions but by integration of the Carnot toolbox [23]. The Carnot toolbox is an extension for MATLAB/Simulink and contains several blocks for the simulation of heating, ventilation and air conditioning systems. Therefore, also blocks for the determination of fluid properties are available in the toolbox. By simply entering the prevailing water-glycol mixture ratio, the fluid properties such as specific heat or density of the HTF are calculated automatically.

$$\begin{bmatrix} \dot{T}_{\mathrm{htf},1} \\ \dot{T}_{\mathrm{pcm},1} \\ \vdots \\ \dot{T}_{\mathrm{htf},N} \\ \dot{T}_{\mathrm{pcm},N} \end{bmatrix} = \begin{bmatrix} \frac{\dot{m}_{\mathrm{htf}} \cdot c_{\mathrm{p,htf},1} \cdot (T_{\mathrm{htf,in}} - T_{\mathrm{htf},1}) + U \cdot (A_{\mathrm{tr}}/N) \cdot (T_{\mathrm{pcm},1} - T_{\mathrm{htf},1})}{\rho_{\mathrm{htf},1} \cdot c_{\mathrm{p,htf},1} \cdot (V_{\mathrm{htf}}/N)} \\ \frac{U \cdot (A_{\mathrm{tr}}/N) \cdot (T_{\mathrm{htf},1} - T_{\mathrm{pcm},1})}{\rho_{\mathrm{pcm},1} \cdot c_{\mathrm{p,pcm},1} \cdot (V_{\mathrm{pcm}}/N)} \\ \vdots \\ \frac{\dot{m}_{\mathrm{htf}} \cdot c_{\mathrm{p,htf},N} \cdot (T_{-\mathrm{htf},N1} - T_{\mathrm{htf},N}) + U \cdot (A_{\mathrm{tr}}/N) \cdot (T_{\mathrm{pcm},N} - T_{\mathrm{htf},N})}{\rho_{\mathrm{htf},N} \cdot c_{\mathrm{p,htf},N} \cdot (V_{\mathrm{htf}}/N)} \\ \frac{U \cdot (A_{\mathrm{tr}}/N) \cdot (T_{\mathrm{htf},N} - T_{\mathrm{pcm},N})}{\rho_{\mathrm{pcm},N} \cdot c_{\mathrm{p,pcm},N} \cdot (V_{\mathrm{pcm}}/N)} \end{bmatrix} \quad (1)$$

where $\dot{m}$ [kg/s] is the mass flow, $c_{\mathrm{p},i}$ [J/(kgK)] and ρ_i [kg/m³] are the specific heat and density of node i, T_i [°C] is the temperature of node i, U [W/(m²K)] and A_{tr} [m²], are the heat transfer coefficient and the heat transfer area and V [m³] describe the volume and finally, N is the total number of discretization nodes. The subscripts "htf" and "pcm" stands for "heat transfer fluid" and "phase change material" respectively.

A fundamental aspect of dynamic modelling of heat flows pertains to the calculation of heat transfer coefficients. In the context of PCM storages, particularly ice storages, the phase transition from liquid to solid and the subsequent formation of an ice layer on the surface of the HEX, is a critical factor influencing the heat transfer coefficient. Due to the much lower thermal conductivity of ice compared to stainless steel, a layer of ice on the surface of the HEX causes a significant drop in the heat transfer coefficient. Studies have shown that the heat transfer coefficients of different types of HEX, become increasingly similar as the ice layer grows [24], [25]. The HEX analysed in this work, consists of four tubes which are connected on the outside by stainless steel plates, see Fig. 3. Taking into account the above-mentioned effect of the ice layer and the associated convergence of the heat transfer coefficients of different types of HEX, the calculation approach outlined in [14] is employed for the HEX presented in this work.

In order to calculate the energy balance and to model the phase transition, knowledge of the specific heat curve of the PCM is required. In [14] the authors use probability density functions to describe the shape of the specific heat curve. This approach enables the determination of the specific heat of the PCM directly through the temperature of the PCM.

Furthermore, by changing the type or adjusting some of the parameters of the probability density function, different types of PCMs can be modelled. The shape of the specific heat curve is therefore derived from adapted logarithmic normal distribution [14]:

$$c_{\mathrm{p,pcm}}(T) = 1000 \cdot \left[a_0 + a_1\left(\varphi(T) - a_2\right)\right], \tag{2}$$

and

$$\varphi(T) = \begin{cases} \dfrac{\exp\left[-\left(\left(\ln\left[-\left(T_{\mathrm{pcm}} - \tau\right)/\gamma\right]\right)^2 / \left(2 \cdot \sigma^2\right)\right)\right]}{-\left(T_{\mathrm{pcm}} - \tau\right) \cdot \sigma \cdot \sqrt{2\pi}}, & T_{\mathrm{pcm}} < \tau \\ 0, & T_{\mathrm{pcm}} \geq \tau \end{cases} \tag{3}$$

where a_0, a_1, a_2, τ, γ and σ are parameters to define the specific heat curve.

Eq. (2) and Eq. (3) are describing the shape of the specific heat curve of the PCM, in the present case of the water/ice system. A detailed description of the modelling approach and values for the individual parameters for defining the specific heat curve can be found in [14].

In order to calculate the SoC of the ice storage, the SoC of the individual nodes of the PCM is calculated first. Since the specific heat curve is given according to Eq. (2) and Eq. (3), the SoC of the individual nodes can be directly determined by integration of the specific heat curve [15]:

$$\mathrm{SoC}_i(T) = \begin{cases} 1 & T_{\mathrm{stm},i} > T_{\mathrm{u}} \\ \dfrac{\int_{T_{\mathrm{l}}}^{T_{\mathrm{stm},i}} c_{\mathrm{p}}(T)\,\mathrm{d}t}{\Delta h_{\mathrm{l}}} & T_l \leq T_{\mathrm{stm},i} \leq T_{\mathrm{u}} \\ 0 & T_{\mathrm{stm},i} < T_{\mathrm{l}} \end{cases}, \tag{4}$$

where SoC_i [–] is the state of charge of node i, $T_{\mathrm{stm},i}$ [°C] represents the temperature of the storge material in node i, T_{u} [°C] and T_{l} [°C] are the upper limit and lower limit temperature defined in the specific heat curve, c_{P} [J/(kgK)] is the specific heat and finally Δh_{l} [J/kg] represents the latent heat of the PCM.

For the upper and lower limit temperature limit of the specific heat curve as well as for the latent heat values for water used in [15] are applied and can be seen in Table 1. Since the SoC- calculation method according to Eq. (4) only considers latent heat and not sensible heat, the SoC can be therefore set equal to the fraction of liquid PCM present. In the case of water serving as PCM, it can be deducted that if the temperature of the PCM is below T_{l}, the PCM is entirely in solid form (ice), whereas at a temperature of T_{u} and above the PCM is completely in liquid form. The calculation of the overall ice storage's SoC is determined by the summation of the individual SoC of all nodes, subsequently divided by the total number of nodes N, according to Eq. (5) [15].

$$\mathrm{SoC}(T) = \frac{\sum_{i=1}^{N} \mathrm{SoC}_i(T)}{N} \tag{5}$$

For modelling the SoC of the ice storage, Eq. (1) to Eq. (5) has been implemented into MATLAB/Simulink. The values used for the simulation and measurement are listed in Table 1.

TABLE 1. PARAMETER USED FOR MODELLING AND MEASUREMENT

Parameter	Abbreviation	Value
Density of HTF	ρ_{HTF}	1033 kg/m^3 (33 vol.% water glycol mixture)
Phase change material	PCM	Water
Heat transfer area	A_{tr}	4.6 m²
Volume flow HTF	$\dot{V}_{htf}$	350 L/h
Total volume of PCM	V_{PCM}	225 L
Total volume of HTF	V_{HTF}	21 L
Number of nodes for simulation	N	20
Lower limit of the specific heat curve	T_l	–5.7 °C
Upper limit of the specific heat curve	T_u	0 °C
Latent heat of the PCM	Δh_l	334 kJ/kg

2.2. Experimental Setup and Analysis

The preliminary experiments are carried out in a stainless-steel storage tank with two spirally formed, steel HEX units (two coils or registers) as shown in Fig. 2. The tank is constructed to contain roughly 400–450 L of water. The distance between the coils is not uniform along the whole HEX, as it is placed roughly centered in the tank. Nevertheless, the coils were initially designed to be approximately 100–110 mm apart along the majority of its length. The aim of this setup is to carry out fast charging/discharging cycles and to determine the influence of the parameters such as fluid medium velocity, flow direction and temperature gradient in the tank on the ice formation on the HEX surface and overall storage functionality. For this purpose, as shown in Fig. 2, four temperature sensors were installed radially between the HEX coils ($T_{1–4}$) and two at the height of each register (T_{top} and T_{bottom}). Further, temperature and volume flow at inlet and outlet of the HEX were registered (T_{in}, T_{out}, $\dot{V}_{in}$ and $\dot{V}_{out}$). The uncertainty of the flowmeter in worst case yields to 0.5 % of reading ±0.1 m/s and those of the temperature sensors range from ±0.15 to ±0.35 K, hence both can be neglected for the purposes of the presented measurements. The capacitive sensor was purchased from HB Products and mounted alongside the HEX as shown in Fig. 2 by the green dashed line. The sensor is developed to detect a (uniform) ice layer growth on a straight pipe for up to 50 mm. According to [26] within the linear range of 0–25 mm, the sensor typically achieves high accuracy with an estimated uncertainty of ±1 mm, while in the 25–40 mm range, uncertainty increases to approximately ±2–3 mm due to reduced sensitivity and nonlinear response. Calibration software was made available from the manufacturer. The sensor's output signal is the precent of the sensor, which is in ice phase, here noted as SoC/%. Although not fully descriptive, the latter labelling was selected to draw attention to the parallels of the results from numerical simulation. As mentioned, the distance between the coils roughly equals twice the detection range (~100 mm) of the capacitive sensor, hence the latter adequately covers the investigated ice layer thickness on one HEX surface.

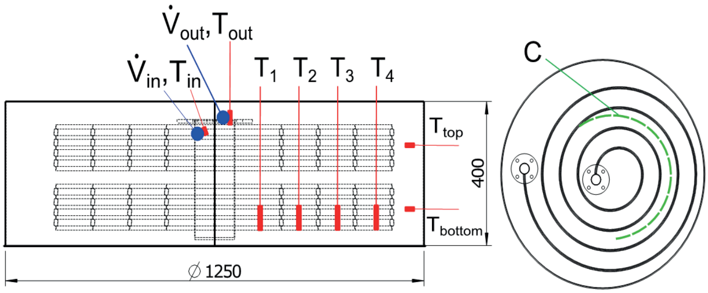

Fig. 2. The placement of temperature sensors: T_1–T_4, T_{in}, T_{out}, T_{top}, T_{bottom} in red; volume flow sensors: $\dot{V}_{in}$ and $\dot{V}_{out}$ in blue; and capacitive sensor in green mounted alongside the HEX (ECOTHERM Austria GmbH, Christof Lehner).

The cooling power is supplied by a water-cooled cooling unit (thermostat) delivering 2–4 kW. A schematic depiction of the hydraulic circuit, consisting of the cooling unit, circulating pumps and a flowmeter is presented in Fig. 3. Generally, the icing first begins at the point where the cold HTF is introduced, which leads to the unidirectional operation modes with the flow directions midpoint (center) to outside point (outwards) of the spiral and vice versa. In order to investigate the ice formation efficiency depending on flow direction and to identify possible optimizations, a hydraulic switchover was developed, which is marked in green dashed rectangle in Fig. 3. The switchover makes it possible to change the flow direction in HEX during the operation, here noted as bidirectional mode. By directly influencing the ice formation and thickness of the layer, an optimized control of the physical processes in the storage tank is enabled.

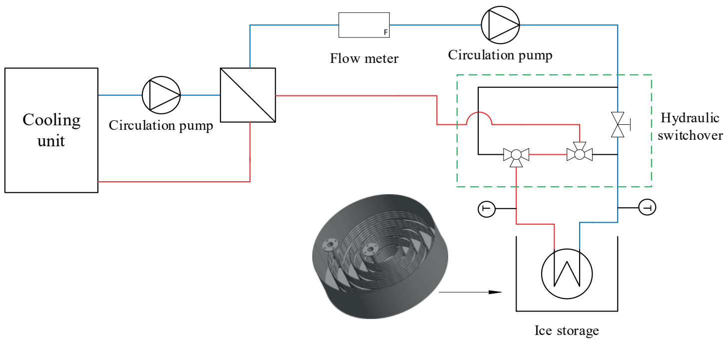

Fig. 3. The hydraulic circuit with integrated ice storage comprised of stainless-steel tank and stainless-steel spiral HEX (ECOTHERM Austria GmbH, Christof Lehner), cooling unit, circulation pumps, flowmeter and hydraulic switchover (green dashed).

3. Results and Discussion

This chapter presents SoC estimation results obtained from the model, as well as the analysis of the experimental data. Further, those results are combined to experimental validation of the SoC model. The correlation of the experimental and numerical work is pointed out in this chapter.

The preliminary icing tests are conducted within fixed temperature and volume flow boundaries. The temperature output of the cooling unit is set to a constant –14 °C and the volume flow to 350 L/h at the beginning of the measurement. Due to lab safety and logistics, the measurement routine is designed to fit in regular working week. The icing cycles are performed during the working days and stopped in the evening, resulting in 8–10-hour cycles of icing and 14–16 hours of uncontrolled de-icing at given room temperature. In order to reduce thermal mixing effects in the HEX and water evaporation, the fluid flow was suspended in the de-icing hours and the tank was loosely covered. A typical measurement week is shown in Fig. 4, where the actual icing days are shaded in blue. For visual clarity, only few representative sensor outputs are depicted in Fig. 4.

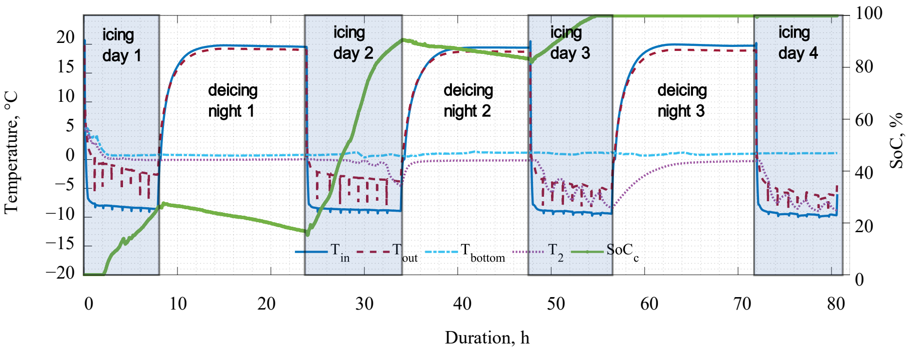

Fig. 4. Exemplary measurement week: bidirectional icing routine with icing days in blue rectangles.

The study focuses on the icing process and couples the ice formation and layer thickness with the SoC determination via changes in permittivity. In contrast to de-icing, icing is a linear process and can be easily controlled by the temperature and volume flow of the system. The de-icing process, on the other hand, is highly dependent on the temperature difference between the HEX surfaces and the water/ice mixture, as well as the quality of ice formation on the HEX surfaces.

Initially, the unidirectional icing process (center outwards) was investigated. On the first day, the energy goes towards cooling down the water in the tank to just above freezing point around 0.5 °C as shown in Fig. 5(a). Additionally, first layer of ice is formed. The capacitive sensor output is depicted by the green solid line in Fig. 5, indicating approximately 38 % of the sensor being in ice phase at the end of the first day. Although the second y-axis is labelled SoC, for the unidirectional measurements with nonuniform ice growth along the HEX, the signal values from the sensor must be put into perspective. As indicated by the sensor output increasing from 27 % to almost 100 %, a substantial amount of ice growth occurs on the second day, see Fig. 5(b). On the third and fourth day the rate of ice growth sinks as the HEX surfaces are covered by ice and the heat flux decreases. The temperature difference ΔT of the HTF yielded to 5.2 °C and 4.7 °C at the end of first and second day, respectively. The corresponding development of the thermal power, as well as the utilized cumulative energy can be observed on Fig. 6. Following temperature differences of 3.3 °C and 3.2 °C were achieved on the third and fourth day. The energy on third and fourth day goes towards lowering the temperature of the existing ice phase down to −6 °C, which comes close the outlet temperature.

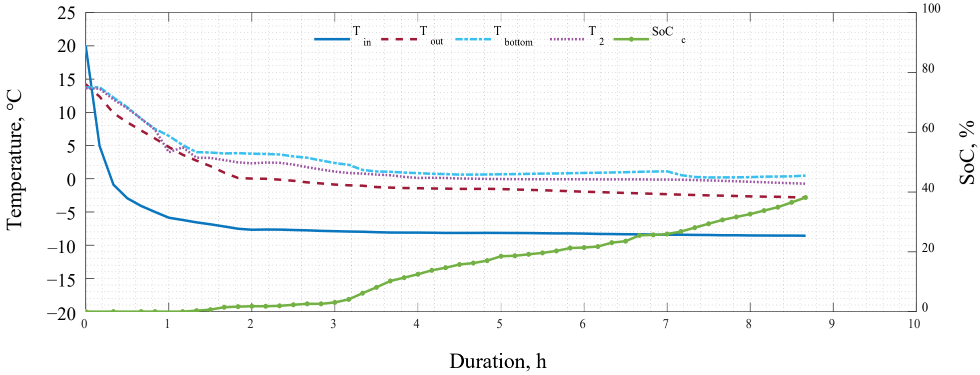

(a)

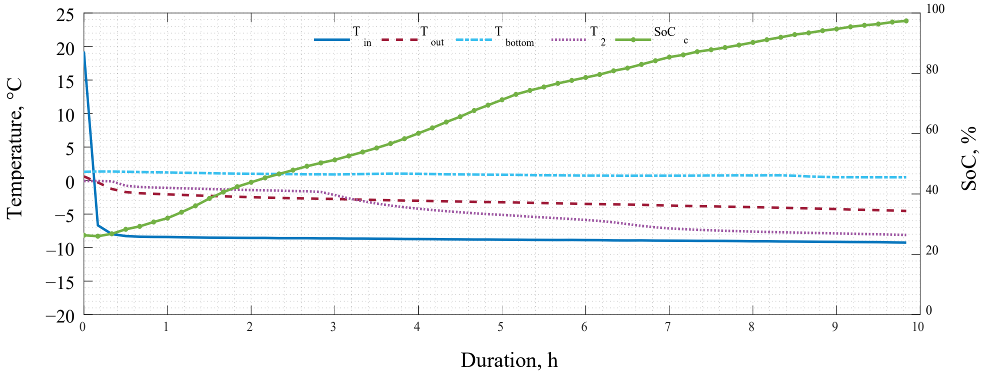

(b)

Fig. 5. Unidirectional icing results (center outwards): a) first and b) second day of icing.

For a complete picture, the thermal power and cumulative energy of every measurement day is plotted in Fig. 6(a) for unidirectional and Fig. 6(b) for bidirectional operational mode corresponding to the data depicted in Fig. 4. Due to the selected mode and uniform ice layer growth, the capacitive sensor readings are lower than those of the unidirectional mode. However, the heat flux and thermal energy calculations for the HEX are found to be highly similar. This demonstrates the importance of sensor placement, calibration and knowledge about the systems configuration.

Fig. 7(a) shows a comparison of the simulated and experimental results with respect to the SoC. The comparison demonstrates a significant agreement between the measured data and the simulation results. For the calculation of the simulated SoC, the average SoC of the nodes 6 to 12 are used, since the capacitive sensor is mounted in between these nodes. The maximum discrepancy observed was found to be −3 %. This deviation occurred after approximately 2 h coinciding with the first icing of the HEX. The simulation indicates that ice formation on the HEX begins after 2 h, while the capacitive sensor registers this after just 1.5 h. Despite this disparity, a high degree of concordance is observed.

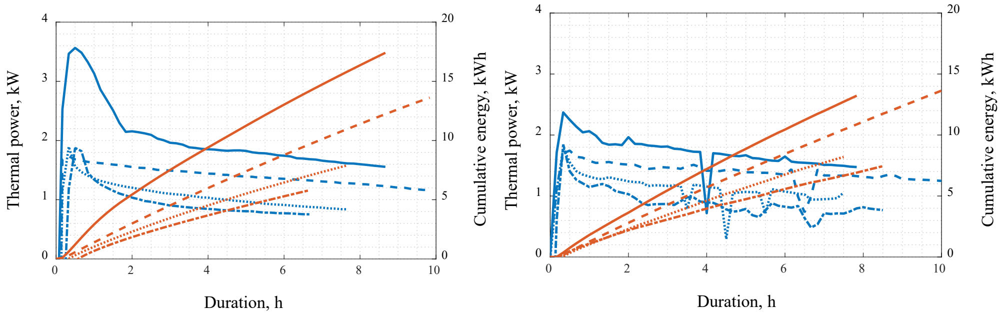

(a) (b)

Fig. 6. Thermal power (blue, left) and cumulative energy (orange, right) of each measurement day: a) unidirectional and b) bidirectional icing.

The comparison of the temperature curves of the ice storage setup and model are presented in Fig. 7(b). As temperature sensor T_2 is placed between two spiral elements of the HEX, the average temperature of the corresponding two nodes is used for a comparison. At the beginning of the icing process a good agreement between the simulation and experimental results is achieved. However, after 1.5 h a small discrepancy is visible, which then decreases after about 4th hour. Regarding the SoC, the effect of the beginning of the icing process is clearly visible here as well. But this effect disappears once a thin layer of ice is formed. For comparison, the average temperature of all nodes was calculated, as shown in Fig. 7(b) and represents therefore the average simulated temperature of the ice storage. The maximum error between the calculated and measured results is 2.5 °C.

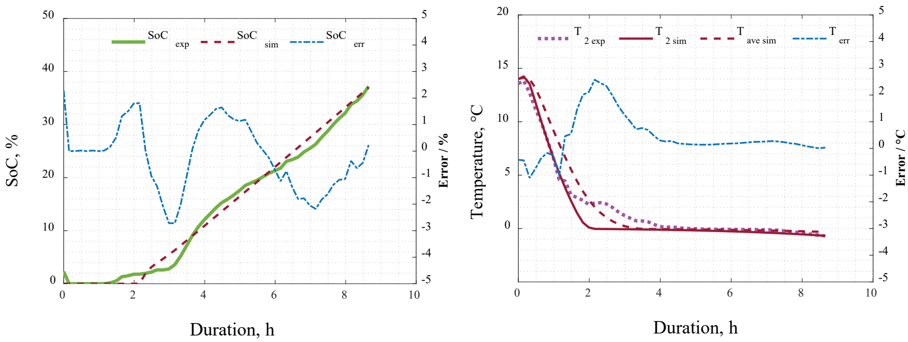

(a) (b)

Fig. 7. Results from the simulation and comparison with measurement data: a) SoC and b) temperature.

4. Conclusion

The adequate state of charge (SoC) determination of latent heat storages, more specifically ice storage, with the purpose of improving control strategies and maximizing their impact is the focus of this paper. Hence, an experimental ice storage setup with steel coil heat exchanger (HEX) equipped with a capacitive sensor was introduced to determine the ice layer thickness.

The experimental efforts were paired with numerical simulations of an ice storage model to describe the SoC of the storage system. This work presents the correlation of the measurements and simulation results.

The ice growth on the HEX surfaces is influenced by the flow direction of the heat transfer fluid (HTF). Hence, a change in the flow direction during the operation was enabled. As for the simulation, the flow direction was kept constant. The initial measurements were carried out in one flow direction from the center outwards, resulting in good agreement between simulation data and capacitive sensor readings. A comparison of the measured and simulated temperatures was also found to demonstrate a high degree of correlation. The main conclusions of the experimental measurements and simulation results are that, although the heat transfer rate is initially high due to the material and configuration of the HEX, the thermal performance decreases significantly after a substantial ice layer has formed.

The bidirectional operation mode was introduced to enforce the formation of a homogeneous and uniform ice layer growth. The latter mode can be one of the operation strategies, which facilitate easier determination of the degree of icing or SoC via capacitive method and subsequently enable a better control of the storage. The experiments resulted in predictable and uniform ice layer growth, which was recorded by the capacitive sensor. The combination of bidirectional icing and capacitive sensing are complementary and deliver more promising results.

Further measurements are planned to investigate the reproducibility of the operation modes and the corresponding control strategies. The development of a capacitive sensor, which can be places alongside the entire length of the HEX is also in progress. Currently, the research group is attempting to test various combinations of methods and pathways to influence ice nucleation and facilitate SoC determination, which will be reported. Additionally, development of de-icing strategies should be considered based on the operation modes in full and partial cycles within the specific application requirements. Further work should be done to describe the bidirectional icing by the numerical method and performing simulations to optimize the entire system, which use ice storages for heating and cooling applications.

ACKNOWLEDGEMENT

This work has been supported by the Government of Upper Austria in the project 'COMPESTO – comprehensive energy storage', Research Grant Wi-2022-600132/7-Au and in the project 'ICE4H&C – ICE Heating and Cooling for SFH and MFH' (FET-Future energy technologies call).

REFERENCES

[1] Vivian J., Heer P., Fiorentini M. Optimal sizing and operation of seasonal ice thermal storage systems. *Energy and Buildings* 2023:300:113633. https://doi.org/10.1016/j.enbuild.2023.113633

[2] Mancin S., Noro M. Reversible Heat Pump Coupled with Ground Ice Storage for Annual Air Conditioning: An Energy Analysis. *Energies* 2020:13(23):6182. https://doi.org/10.3390/en13236182

[3] Merve Altuntas and Dogan Erdemir. An investigation on potential use of ice thermal energy storage system as energy source for heat pumps. *Journal of Energy Storage* 2022:55:105588. https://doi.org/10.1016/j.est.2022.105588

[4] Carbonell D., Philippen D., Haller M. Y., Brunold S. Modeling of an ice storage buried in the ground for solar heating applications. Validations with one year of monitored data from a pilot plant. *Solar Energy* 2016:125:398–414. https://doi.org/10.1016/j.solener.2015.12.009

[5] Chengjun Li *et al.* Dynamic heat transfer characteristics of ice storage in smooth-tube and corrugated-tube heat exchangers. *Applied Thermal Engineering* 2023:223:120037. https://doi.org/10.1016/j.applthermaleng.2023.120037

[6] Colangelo A., Guelpa E., Lanzini A., Mancò G., Verda V. Compact Model of Latent Heat Thermal Storage for Its Integration in Multi-Energy Systems. *Applied Sciences* 2020:10(24):8970. https://doi.org/10.3390/app10248970

[7] Steinmaurer G., Krupa M., Kefer P. Development of Sensors for Measuring the Enthalpy of PCM Storage Systems. *International Conference on Solar Heating and Cooling for Building and Industry*, September 23–25, 2013, Freiburg, Germany. https://doi.org/10.1016/j.egypro.2014.02.052

[8] Ezan M. A., Çetin L., Erek A. Ice thickness measurement method for thermal energy storage unit. *DergiPark* (Istanbul University). https://dergipark.org.tr/tr/pub/isibted/issue/33980/376134

[9] Zsembinszki G., Orozco C., Gasia J., Barz T., Emhofer J., Cabeza L. F. Evaluation of the State of Charge of a Solid/Liquid Phase Change Material in a Thermal Energy Storage Tank. *Energies* 2020:13(6):1425. https://doi.org/10.3390/en13061425

[10] Tiwari V., Rai A. C., Srinivasan P. Parametric analysis and optimization of a latent heat thermal energy storage system for concentrated solar power plants under realistic operating conditions. *Renewable Energy* 2021:174:305–319. https://doi.org/10.1016/j.renene.2021.04.073

[11] Ajarostaghi S. S. M., Poncet S., Sedighi K., Delavar M. A. Numerical Modeling of the Melting Process in a Shell and Coil Tube Ice Storage System for Air-Conditioning Application. *Applied Sciences* 2019:9(13):2726. https://doi.org/10.3390/app9132726

[12] Barz T. *et al.* State and state of charge estimation for a latent heat storage. *Control Engineering Practice* 2018:72:151–166. https://doi.org/10.1016/j.conengprac.2017.11.006

[13] Mehmood T., Shah N. u. H., Ali M., Biwole P. H., Sheikh N. A. Simplified mathematical model and experimental analysis of latent thermal energy storage for concentrated solar power plants. *Journal of Energy Storage* 2021:41:102871. https://doi.org/10.1016/j.est.2021.102871

[14] Bastida H., Ugalde-Loo C. E., Abeysekera M., Jenkins N. Dynamic modelling of ice-based thermal energy storage for cooling applications. *IET Energy Systems Integration Volume* 2022:4(3)317–334. https://doi.org/10.1049/esi2.12061

[15] Bastida H., de La Cruz-Loredo I., Ugalde-Loo C. E. Effective estimation of the state-of-charge of latent heat thermal energy storage for heating and cooling systems using non-linear state observers. *Applied Energy* 2023:331:120448. https://doi.org/10.1016/j.apenergy.2022.120448

[16] Zhi X., Cho H. C., Wang B., Ahn C. H., Moon H. S., Go J. S. Development of a capacitive ice sensor to measure ice growth in real time. *Sensors (Basel, Switzerland)* 2015:15(3):6688–6698. https://doi.org/10.3390/s150306688

[17] Owusu K. P., Kuhn D. C., Bibeau E. L. Capacitive probe for ice detection and accretion rate measurement: Proof of concept. *Renewable Energy* 2013:50:196–205. http://doi.org/10.1016/j.renene.2012.06.003

[18] Artemov V. G., Volkov A. A. Water and Ice Dielectric Spectra Scaling at 0°C. *Ferroelectrics* 2014:466(1):158–165. https://doi.org/10.1080/00150193.2014.895216

[19] Artemov V. G., Ryzhkin I. A., Sinitsyn V. V. Similarity of the dielectric relaxation processes and transport characteristics in water and ice. *JETP Letters* 2015:102(1):41–45. https://doi.org/10.1134/S0021364015130020

[20] Dou Y., Qin J., Chang X. The Study of a Capacitance Sensor and its System Used in Measuring Ice Thickness, Sedimentation and Water Level of a Reservoir. In *International Forum on Information Technology and Applications*, Chengdu, China, 2009. https://doi.org/10.1109/IFITA.2009.79

[21] Volkov A. A., Vasin A. A. Dielectric properties of water and ice: a unified treatment. *Ferroelectrics* 2019:538(1):83–88. https://doi.org/10.1080/00150193.2019.1569989

[22] Cyril, B. K., Boby, G. A capacitive sensing system for Non-Contact: detection of ice. *International Journal on Smart Sensing and Intelligent Systems* 2014:7(5):1–6. https://doi.org/10.21307/ijssis-2019-098

[23] CARNOT Toolbox Ver.8.02 for Matlab/Simulink R2021b, © Solar-Institut Jülich.

[24] Philippen D., Logie W., Thalmann M., Haller M. Y., Brunold S., Elimar F. Development of a heat exchanger that can be de-iced for the use in ice stores in solar thermal heat pump systems. *EuroSun2012*, *ISES-Europe Solar Conference*, Rijeka, Croatia, 18–20 September 2012.

[25] Carbonell D., Philippen D., Haller M. Y., Frank E. Development and Validation of a Mathematical Model for Ice Storages with Heat Exchangers that can be De-iced. *Energy Procedia* 2014:57:2342–2351. https://doi.org/10.1016/j.egypro.2014.10.242

[26] HB Products, Ice bank sensor – product description and datasheet 2022. [Online]. [Accessed 08.09.2025]. Available: https://www.hbproducts.dk/images/product_files/Datasheets/Ice_Bank_Sensor.pdf